FABRICATION AND CHARACTERIZATION OF MICROCALCIFICATION BREAST PHANTOM FOR IMAGE QUALITY ANALYSIS

OKOH FRANCA OYIWOJA

UNIVERSITI SAINS MALAYSIA

2022

FABRICATION AND CHARACTERIZATION OF MICROCALCIFICATION BREAST PHANTOM FOR IMAGE QUALITY ANALYSIS

by

OKOH FRANCA OYIWOJA

Thesis submitted in fulfillment of the requirements
for the degree of
Doctor of Philosophy

October 2022

ACKNOWLEDGEMENT

I wish to appreciate the Almighty God for granting me the grace and ability to complete my PhD study. I would like to thank my main supervisor Dr Norlaili Ahmad Kabir for her tireless support and guidance throughout my PhD journey. This thesis would not have been possible without her help. I would also like to express my gratitude to my co-supervisor, Dr Mohd Fahmi Mohd Yusof for his supervision, advice, and guidance throughout my study. I sincerely appreciate Dr Ahmad Sufril Azlan Mohammed who co-supervised my research, for his insightful suggestions and comments. I wish to also acknowledge Associate Professor Dr Rafidah Zainon who has contributed in co-supervising my PhD. Special thanks go to all staff of the laboratories in the School of Physics, Centre for Global Archaeological Research, Radiology Departments of Hospital Universiti Sains Malaysia (HUSM), and the Advanced Medical and Dental Institute (AMDI) USM, who have assisted me in conducting my experiments in a specific manner. I am grateful to Federal University Wukari, Nigeria for granting me the opportunity to undertake a PhD program. My gratitude is extended to those, who helped and contributed to this study through their great ideas and ample advice, especially Mr. Hazhar Hassan, Mr. Mohd Rizal Mohd Rodin, Mrs Siti Nor Azizah Abdullah, Dr Hafidz Jafar, and Dr Niri Matha Choji. Special thanks go to my husband Dr Umale Okoh who is the major pillar of support behind my success, my kids Oche Emmanuel Okoh and Agbenu Faithful Okoh for their sacrifice and having to cope with my busy schedule these past few years. I wish to sincerely acknowledge my father Mr A. A Ujah of blessed memory, and my beloved mother Mrs Jenebu Ujah for laying the foundation for what I have become today. I appreciate all my brothers and sisters for their constant support and encouragement, thank you so much for being a part of my life, I am profoundly grateful. Finally, I wish to acknowledge all my colleagues and those who supported me in any aspect during my research. I apologise that I could not mention all of you one by one.

TABLE OF CONTENTS

LIST OF TABLES

Page

LIST OF FIGURES

Page

LIST OF SYMBOLS AND ABBREVIATIONS

ρ	Density
ρ_{eff}	Effective electron density
μ	Linear Attenuation Coefficient
μ/ρ	Mass Attenuation Coefficient
^{241}Am	Americium-241
AAPM	American Association of Physicists in Medicine
AEC	Automatic Exposure Control
ANOVA	Analysis of Variance
BIRADS	Breast Imaging Reporting and Data System
$CaCO_3$	Calcium Carbonate
CAD	Computer Aided Diagnostic
CIRS	Computerized Imaging Reference System
Cn	Contrast
CNR	Contrast-to-Noise Ratio
CT	Computed Tomography
DICOM	Digital Imaging and Communications in Medicine
ESD	Entrance Surface Dose
FESEM	Field Emission Scanning Electron Microscope
HU	Hounsfield Unit
ICRU	International Commission on Radiation Units and Measurements

keV	Kiloelectron Volt
kVp	Peak Kilovoltage
mAs	Tube Current Time
MC	Microcalcification
MCs	Microcalcifications
MGD	Mean Glandular Dose
MSE	Mean square error
OSLD	Optically Simulated Luminescence Dosimeter
PSNR	Peak signal to noise ratio
PVAL	Polyvinyl alcohol
SNR	Signal to noise ratio
Stdev	Standard Deviation
TLD	Thermoluminescence Dosimeter
XCOM	Photon Cross Sections Database
Z_{eff}	Effective Atomic Number

PEMFABRIKASI DAN PENCIRIAN FANTOM MIKROKALSIFIKASI PAYUDARA UNTUK ANALISIS KUALITI IMEJ

ABSTRAK

Kajian ini bertujuan untuk menambah baik diagnosis awal kanser payudara melalui aplikasi teknik pemprosesan imej berdasarkan algoritma MATLAB untuk meningkatkan keterlihatan mikrokalsifikasi dalam Mamografi Digital Medan Penuh (FFDM). Pelbagai fantom komposit polivinil alkohol (PVAL) telah dihasilkan untuk membina persekitaran fizikal dan radiologikal bagi kategori tisu payudara yang berbeza selaras dengan klasifikasi BIRADS. Ketumpatan, komposisi unsur, nombor atom berkesan (Z_{eff}), ketumpatan elektron ($ƒ_{eff}$), dan pekali pengecilan jisim bagi fantom berasaskan PVAL dan ciri mikrokalsifikasi ($CaCO_3$/grafit) telah ditentukan. Struktur mikro dan nombor CT bagi PVAL juga ditentukan. PVAL 50/50 air/etanol 10 wt% PVAL (E50), 10 wt% PVAL berasaskan air (P10), 10 wt% PVAL dicampur dengan 4% serbuk grafit (G4), dan fantom berbeza yang telah dihasilkan mempunyai sifat fizikal dan radiologi yang menyamai kategori tisu payudara BIRADS B, C, D. Fantom E50, P10, G4 dan H mencatatkan ketumpatan 0.952 ± 0.011, 1.056 ± 0.002, 1.081 ± 0.002, dan 1.025 ± 0.006 g/cm^3, julat Z_{eff} dari 7.148 hingga 7.418 dan julat $ƒ_{eff}$ dari 3.189 hingga 3.209 ×10^{23}/g. Nombor CT mempunyai julat dari -21.40 hingga 24.13 HU bagi E50 dan G4, yang mana masing-masing adalah paling rendah dan tertinggi. Pekali pengecilan jisim phantom dan mikrokalsifikasi (MC) menyamai nilai sperti keputusan simulasi. Nilai Kontras (Cn), nisbah kontras ke bunyi (CNR) dan nisbah isyarat ke bunyi (SNR) yang lebih tinggi telah direkodkan untuk fantom dengan ketumpatan yang lebih rendah (E50 dan H) terutamanya pada tiub voltan yang lebih rendah iaitu 26 kVp. Analisis saiz dan kedalaman MC menunjukkan kesan yang sedikit tetapi tidak ketara bagi nilai Cn, CNR, dan SNR untuk 3 kedalaman MC yang berbeza. Purata dos kelenjar (MGD) didapati meningkat dengan peningkatan

kepadatan dan ketebalan fantom payudara. Mamogram yang diperoleh pada 30 kV menghasilkan MGD paling sedikit dengan kualiti imej yang boleh mencukupi. Dos yang direkodkan adalah konsisten dengan nilai yang diterbitkan dan piawaian Kolej Radiology Amerika (ACR). Penyingkiran Gaussian mencatatkan prestasi terbaik dari segi penilaian kualitatif bagi penampakkan MC. Secara kuantitatif, penapis median, operasi morfologi pembukaan, dan penyingkiran Gaussian merekodkan MSE yang lebih rendah dan nilai PSNR yang lebih tinggi berbanding dengan penapis lain yang digunakan. Kajian ini boleh disimpulkan bahawa fantom E50, P10, G4, dan H boleh berfungsi sebagai bahan fantom payudara yang berpotensi untuk dosimetri dan kajian kualiti imej dalam mamografi.Fantom yang telah dihasilkan telah digunakan dalam aplikaksi penyingkiran Gaussian dan operasi morfologi pembukaan dan kajian tersebut menunjukkan peningkatan kualiti kualitatif dan kuantitatif imej mikrokalsifikasi pada mamogram.

FABRICATION AND CHARACTERIZATION OF MICROCALCIFICATION BREAST PHANTOM FOR IMAGE QUALITY ANALYSIS

ABSTRACT

This study aims to improve the early diagnosis of breast cancer through the application of image processing techniques based on the MATLAB algorithms to enhance the visibility of microcalcifications (MCs) in Full Field Digital Mammography (FFDM). Various polyvinyl alcohol (PVAL) composites phantoms were produced through freezing and thawing method to mimic the physical and radiological properties of different categories of breast tissue in line with the BIRADS classification. The density, elemental composition, effective atomic number (Z_{eff}), electron density ($ƒ_{eff}$), mass attenuation coefficients of the PVAL-based phantoms and MC features ($CaCO_3$/graphite) were determined. The microstructure and CT number of the PVAL were also studied. The 50/50 water/ethanol-based 10 wt% PVAL (E50), the water-based 10 wt% PVAL (P10), 10 wt% PVAL mixed with 4% graphite powder (G4), and the heterogeneous phantom (H) had physical and radiological properties suitable to mimic BIRADS B, C, D, and a heterogeneous breast tissue respectively. Phantom E50, P10, G4, and H recorded densities of 0.952 ± 0.011 g/cm^3, 1.056 ± 0.002 g/cm^3, 1.081 ± 0.002 g/cm^3, and 1.025 ± 0.006 g/cm^3 respectively, their Z_{eff} and $ƒ_{eff}$ ranged from 7.148 to 7.418 and 3.189 X 10^{23}/cm^3 to 3.209 X 10^{23}/cm^3 respectively. The CT number ranged from -21.40 to 24.13 HU with E50 and G4 being the least and highest respectively. The mass attenuation coefficients of phantoms and MCs agreed with tissue values acquired via simulation studies. Significantly higher contrast (Cn), contrast to noise ratio (CNR), and signal to noise ratio (SNR) values were recorded for phantoms with lower densities (E50 and H) especially at lower tube voltage (26 kVp). Analysis of MC size and depth showed a slight but insignificant variation in the

values of Cn, CNR, and SNR for the 3 different depths of MCs studied. The mean glandular dose (MGD) were found to increase with an increase in breast phantom density and thickness. Mammograms acquired at 30 kV yielded the least MGD with acceptable image quality. Recorded doses were consistent with published values and ACR standard. Gaussian elimination recorded the best performance in terms of qualitative assessment of MC visibility. Quantitatively, the median filter, opening morphological operation, and Gaussian elimination recorded lower mean square error (MSE) and higher peak signal to noise ratio (PSNR) values. This study concluded that the E50, P10, G4, and H could serve as potential breast phantom materials for dosimetry and image quality study in mammography. The fabricated phantoms were employed to study Gaussian elimination and the opening morphological operation pre-processing filters where the results showed improved visibility of MCs on mammograms, qualitatively and quantitatively.

CHAPTER 1 INTRODUCTION

1.1 Introduction

Microcalcifications (MCs) are tiny calcium deposits present in breast tissue with diameter less than or equal to 1 mm. They are found in about 30% of all malignant breast lesions, in 50% of nonpalpable malignant breast lesions, and constitute 85 to 95% of all cases of ductal carcinoma in-situ in screening campaigns. Generally, large MCs of about 1 mm diameters are often benign while those under 0.5 mm are mostly associated with malignancy. Although, there are exceptions since coarse heterogeneous or dystrophic calcifications with diameters greater than 1 mm may also relate to malignant lesions (Henrot et al., 2014).

Mammography is an acceptable standard test for the early detection of breast cancer but it is not an ideal procedure (Ciraj-Bjelac et al., 2012; Lee et al., 2019; O'Grady & Morgan, 2018; Tahiri et al., 2021). One of the major limitations of mammography is false-negative diagnosis i.e. cases of breast cancer where radiologists fail to rule out diagnosis. It is estimated that 13% of women undergoing annual mammogram testing to screen for breast cancer have the false-negative diagnosis (Basile et al., 2019). The identification of MC on mammogram is quite demanding, not only because of the wide difference in breast composition and greatly textured breast anatomy, but also because of the inherent low contrast of mammograms and, in many instances, the impalpable size of MCs. Visible cancers are missed for several reasons at routine mammography, and their number could likely be reduced. Surely, the radiologists' sense of perception is responsible for the false-negative rate (Destounis et al., 2004), because even the most experienced of radiologists might miss cancers that are visible in retrospect, because of the radiologists' inability to perceive worrisome lesions, subtle or not (Destounis et al., 2004). The image quality of any mammogram is key in the diagnosis of breast cancer. The ability to distinguish between MCs and dense breast tissues on a mammogram

is extremely important because MCs and dense breast are presented with overlapping intensity distribution due to their close attenuation values (Gazi et al., 2015).

When calcifications are not resolved at the early stage, it may lead to severe consequences where patients with malignant calcifications may suffer more harm which could result in grievous outcomes. Prior studies of the repercussion of delay on prognosis for women with breast cancer demonstrated that increased delay is related to more advanced stage cancers at diagnosis, thus resulting in lower chances of survival (Caplan et al., 2014; Unger-Saldaña, 2014; L. Wang, 2017). Generally, breast cancer cells tend to grow and divide more rapidly than normal healthy cells. This rapid growth process causes the cells to form a mass or a lump that can spread from the breast area to the lymph nodes resulting in cancer metastasis.

Recent study show that the integration of digital mammography systems and the application of computer-aided detection (CAD) technique has allowed for an improvement in the assessment of MCs long before they become an actual lump (Hernández et al., 2016; Basile et al., 2019; Tripathy & Swarnkar, 2020). This explains why developed countries engage in regular breast cancer screening for women above age 40. The MATLAB software is one of the general-purpose commercial software commonly employed for the implementation of image processing algorithms. Even though MATLAB users can develop their own algorithms to suit specific purposes, the MATLAB Image Processing Toolbox (IPT) provides an extensive set of reference-standard algorithms and workflow applications for image processing, analysis, and visualization. The IPT application allows automation of common image processing workflows. It can be used to perform image segmentation, image enhancement, noise reduction, geometric transformations, image registration and 3D image processing operations (MathWorks, 2012).

This research was embarked with an aim to produce tissue equivalent breast phantoms for the purpose of studying the effect of MATLAB based image processing techniques on visibility and detection of MCs on mammograms acquired via Full Field Digital Mammography (FFDM). Scanning breast phantoms that were fabricated with similar physical and radiological values as to breast tissues will provide similar radiation attenuation as to how x-ray photons interact with breast tissue. In this study, the breast phantom is the key to provide accurate image processing results in response to various problem statements in regards to visibility of MCs on mammograms.

1.2 Problem statement

Commercial phantoms are widely available for use in simulating breast tissues. However, while these phantoms are efficient for characterizing the innate physical properties of an imaging system, they were not built with realistic physical properties that are consistent with actual breast tissue, thereby falling short of diagnostic functions that should be the fundamental of medical imaging performance (Kiarashi et al., 2015). Additionally, commercial phantoms are constituted for broad markets and specific applications and are not customizable. Hence, customized design and construction of tissue equivalent phantoms are needed for specific applications that require tailored properties or dimensions, and in a bid to reduce cost. The poly vinyl alcohol (PVAL) breast phantom designed by Price and his colleagues could be utilised in this research because of their compressive nature as mammography require compression (Price et al., 2010a). However, the PVAL/ethanol breast phantom by Price et al. (2010a) has no embedded calcifications. Moreover, it represents only one category of breast tissue (BIRADS B). This present study requires additional phantoms that mimic dense breast tissues (BIRADS C and D). Therefore, this study is carried out to fabricate and develop physical and radiological properties of PVAL based tissue equivalent phantoms of various densities that can be used to simulate breast tissue and MCs.

Distinguishing between MCs and dense breast tissues on mammograms is demanding because of their close attenuation properties. MCs appear whitish on mammograms just like dense breast tissue, this poses a great difficulty in detecting MCs in dense breast tissues at its early stage. Dense breasts contain over 50% fibro glandular tissues and tends to mask the abnormal tissues leading to a difficulty in interpreting mammograms of young women with greater mammographic breast density. Inasmuch as mammography has been proven to be a useful tool in the early diagnosis of breast cancer, the accurate interpretation of mammograms can sometimes be a challenge (Dheeba et al., 2014). It requires differentiation of soft tissues with small difference in x-ray attenuation and visualization of small, irregularly shaped calcification. Consequently, subtle details such as the presence of MCs located within high density tissue cannot be easily detected. Even the most experienced radiologists can miss subtle variations in tissue that might constitute worry. To optimize the benefits of a mammography examination, the system must operate under extremely controlled technical conditions, yielding the necessary image quality at the lowest radiation dose possible. In mammography, the benefit is expressed by image quality parameters such as contrast (Cn), contrast to noise ratio (CNR), and signal to noise ratio (SNR), while the risk is associated with the mean glandular dose (MGD). (D13) This study is carried out to evaluate the factors that influence image quality in mammography.

One of the factors underpinning the investigation of the risks-benefits of mammography is the accurate knowledge of the absorbed dose since it is established that there is a relationship between breast dose and breast cancer. Mammograms with acceptable diagnostic qualities should be acquired with a radiation dose as low as possible. Image quality and dose depend largely on the breast characteristics (glandularity and thickness) and the set of exposure parameters such as the peak kilovoltage (kVp), tube current-time (mAs), anode-filter combination, and compression force), used for scanning (Chevalier et al., 2012). The low energy x-ray beam

(specified by the kVp and the anode-filter combination) essential for visualizing subtle density differences between normal and abnormal tissues has a significant role in image quality and absorbed radiation dose. Increasing the kVp leads to an increase in the efficiency and output for a specific mAs value, it also shifts the photon energy spectrum upward so that the beam becomes more penetrating, and the dose is reduced. Conversely, x-ray beams that have lower average photon energy increase the breast dose. In past studies, the use of the optimized Tungsten/Rhodium (W/Rh) technique compared to standard Molybdenum/Molybdenum (Mo/Mo) techniques with a commercial phantom provided dose savings ranging from 9% for 2 cm thickness, 100% adipose breasts, to 63% for 6 cm thickness, 100% glandular breasts, and for breasts with a 50% adipose/50% glandular composition, from 12% for 2 cm breast thickness up to 57% for 8 cm breast thickness (Ranger et al., 2010). In a similar study, Baldelli and his colleagues (Baldelli et al., 2010), compared two digital mammography units; one unit utilises Mo/Mo and Mo/Rh as target/filter combinations, while the other unit uses W/Rh and Tungsten/Silver (W/Ag). The least dose and best image quality were recorded for W/Rh combination at 28 kV. Moreover, the system with Tungsten (W) anode demonstrates a better optimisation of the automatic exposure control in comparison with the system with Mo anode. However, the comparison of MGD and corresponding image quality at 26 - 28 kVp (auto mAs) for different densities of fabricated PVAL based breast phantoms have not been carried out. This study is carried out to ascertain how image acquisition parameters affect dose in customised and low-cost PVAL based phantoms that mimic various densities of breast tissues for dose and image quality study.

The inherent blurring and low contrast that characterize mammograms contribute to poor image quality. Blurring is principally noteworthy in mammography due to the need to image MCs. This is because blurring reduces the sharpness and spatial resolution of the tiny MCs thereby constituting a great difficulty to radiologists in visualizing MCs on mammograms due to their small size which could lead to

late/missed diagnosis and consequently, poor prognosis. The use of image processing algorithm provides the maximum possible amount of beneficial information available on the mammogram to the radiologists. Thus, the visual appearance of the mammogram is modified, thereby producing an improved visibility of the normal breast structures and abnormalities for a human reader, by optimising the displayed brightness and contrast throughout the image (Boita et al., 2021). Therefore, this study is embarked upon to enhance the image quality and early detection of MC at a low dose through the application of image processing technique.

1.3 Research objectives

The research objectives are as follows:

1. To evaluate the physical properties, effective atomic number, electron density, CT number, and attenuation coefficients of fabricated PVAL based breast equivalent phantoms mimicking BIRADS category B, C, D and a heterogeneous breast.

2. To analyse the effect of breast density, microcalcification (MC) size and depth, phantom compositions, and scanning parameters on image quality and mean glandular dose (MGD).

3. To evaluate the image quality metrics when mammograms are enhanced using image processing techniques based on MATLAB algorithm.

4. To propose the best scanning parameters and matching MATLAB algorithms for optimum image quality and dose in MC imaging.

1.4 Scope of research

Owing to the limitations of available phantoms, this research fabricated breast tissue equivalent phantoms based on PVAL with embedded MCs to mimic breast tissues of various densities according to BIRADS classification (D'Orsi et al., 2016). The phantoms which possess physical and radiological properties equivalent to breast tissue were utilized for FFDM imaging at clinical protocol. The image quality of

original mammograms were assessed by measuring the noise, contrast, CNR and SNR values at different acquisition parameters using ImageJ. The effect of image acquisition parameters on dose were evaluated. Furthermore, the acquired mammograms were subjected to digital image processing based on MATLAB algorithm to improve MC visibility and contrast, more so, the processed images were evaluated qualitatively and quantitatively. The qualitative analysis was based on visual perception while the quantitative methods employed image quality metrics (IQM) namely, the mean square error (MSE), peak signal to noise ratio (PSNR), CNR, SNR and noise. Finally, the best scanning parameters and matching MATLAB algorithms for optimum image quality and dose in MC imaging was selected.

1.5 Thesis Structure

This thesis consists of 5 chapters. Chapter 1 explains breast cancer, MCs and the method used for early diagnosis. This chapter also discussed the problem statements, aim and objectives of the research work together with the scope of the thesis.

Chapter 2 contains the theoretical background, the basic principles of X-ray mammography was described, followed by a literature review of relevant studies. Chapter 3 discusses the materials and methods employed in the research. This involved the fabrication of the PVAL composite gels and MC features and testing of their physical and attenuation properties. In addition, the method of fabrication of the breast phantoms and scanning procedure were described. The image processing techniques applied to enhance the quality of the image and the image quality metrics employed to assess their performance were also discussed in this chapter.

Chapter 4 discusses the results of all experiments performed in this study: the acquired results for the physical and attenuation properties of fabricated phantoms and calcifications were presented. This was followed by the analysis of image quality, ESD and MGD of acquired mammograms. The acquired images were filtered and post processed based on MATLAB algorithms. Moreso, the quality of images

achieved were assessed both qualitatively and quantitatively. Finally, the conclusion of this thesis is presented in Chapter 5. The recommendations for future works are also stated in this Chapter.

CHAPTER 2 THEORY AND LITERATURE REVIEW

This chapter aims to discuss the anatomy of human breast and breast cancer. It also focuses on the overview of the role of breast phantoms in the diagnosis of breast cancer and patient dose evaluation in digital mammography. Furthermore, the application of computer-aided diagnosis (CAD) in mammography is also discussed.

2.1 Theory

2.1.1 Mammography x-ray

Mammography utilizes low-energy x-rays to produce 2 or 3D images of the breast tissue for screening or diagnostic purposes. The x-ray spectrum employed in this procedure has a vital effect on the image quality and radiation dose to patients (Sprawls, 1995).

2.1.1(a) Mammography x-ray tube

X-rays are produced in the x-ray tube (Figure 2.1) when fast-moving electrons collide with the anode material and are decelerated. An x-ray tube is mainly composed of the anode, cathode, and glass envelop. The cathode serves as the negative terminal of the x-ray tube, it is made up of a tungsten filament which allows current to flow through it thereby heating it up. The heated filament emits its surface electrons through thermionic emission. The anode is the positive terminal of the x-ray tube. Most mammography anodes are made of molybdenum, although rhodium and tungsten are also used. The fast-moving electrons from the cathode move toward the positively charged anode terminal and strike the target material with high energy determined by the applied kilovoltage. This leads to the production of heat and x-ray. The process of generating the x-ray beam is overly ineffective, with 99% of the electrical energy being converted into heat and only 1% of the electrical energy converted into x-rays. The x-ray photons are released out of the window of the x-ray tube.

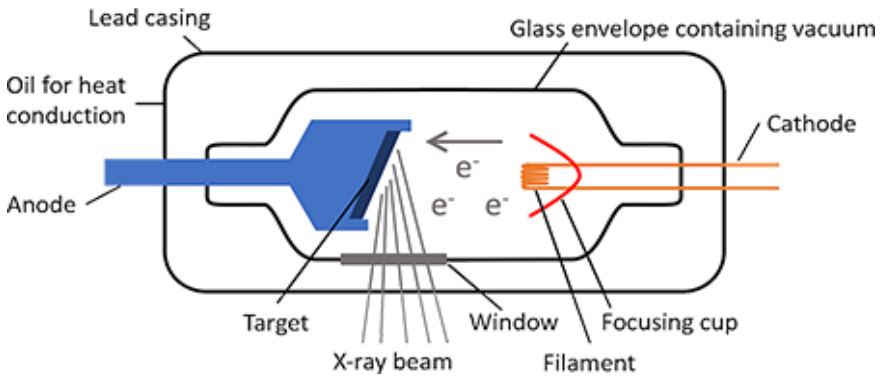

Figure 2.1 Schematic diagram of x-ray tube (Abdulla, 2020)

The configuration of the x-ray tube such as focal spot size, x-ray field uniformity, and the x-ray energy spectrum determines the properties of the x-ray beam. These x-ray beam properties are crucial as they influence radiologic variables like spatial resolution, image contrast, and patient dose. In mammography, small focal spot sizes are often used (0.3 mm) to improve spatial resolution. The relative composition of the x-ray spectrum generated in mammography in respect of bremsstrahlung and characteristic radiation depends on the applied maximum kilovoltage and the anode/filter combination used.

Table 2.1 shows the characteristic and K edge energies for target/filter combinations used in mammography. The target/filter combination commonly used in mammography is either the molybdenum/molybdenum (Mo/Mo) or molybdenum/rhodium (Mo/Rh) combination. However, some mammography units possess dual anode and/or filters. This permits manual or automatic selection of either molybdenum or rhodium by the radiographer or AEC respectively (Sprawls, 1995). Furthermore, because of the features of the new digital detectors, other target/filter combinations which have some advantages for imaging dense breast could be used. Such target/filter combinations include rhodium/rhodium (Rh/Rh), tungsten/rhodium (W/Rh), tungsten/silver (W/Ag) and tungsten/aluminium (W/Al). The breast doses and contrast are associated with these combinations are lower than those delivered with Mo/Mo or Mo/Rh (Chevalier et al., 2012).

Table 2.1 Characteristic and K-edge energies for common target/filter combinations used in mammography

Target/filter combination	Characteristic x-ray of target (keV)	K-edge of Filter (keV)
Mo/Mo	17.5 and 19.7	20
Mo/Rh	17.5 and 19.7	23.2
Rh/Rh	20.2 and 22.8	23.2
W/Rh	59.3	23.2
W/Ag	59.3	25.5
W/Al	59.3	1.6

Figure 2.2 shows the x-ray spectra at 30 kVp for Mo/Mo (a), Mo/Rh (b), Rh/Rh (c), and W/Rh (d) target/filter combinations. Mammography units are provided with unique anode/filter combinations to operate in the appropriate kVp range. Naturally, breast tissues are lacking in subject contrast, requiring the use of low energy x-ray spectra, which emphasize the compositional differences of the breast tissues (NCRP, 2005).

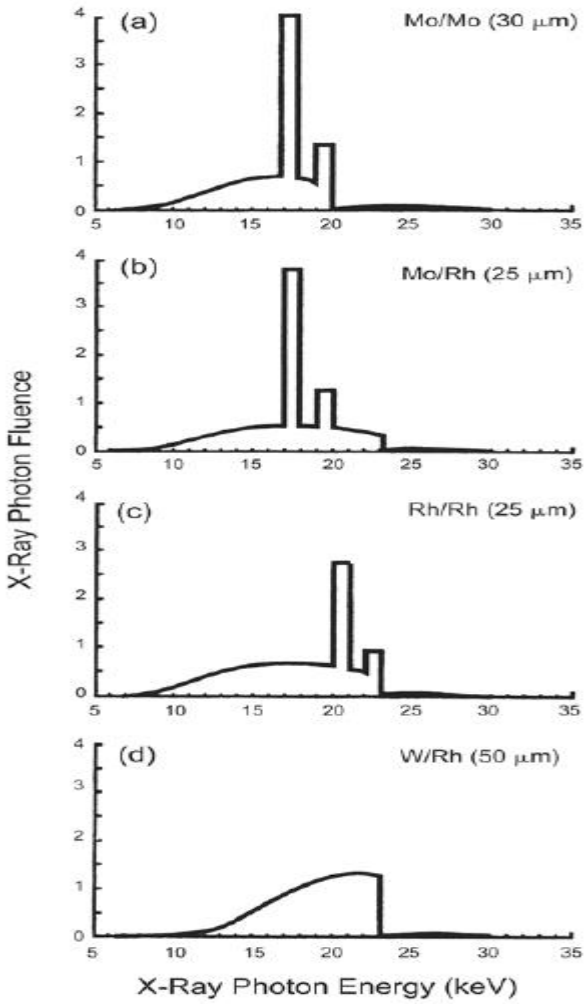

Figure 2.2 X-ray spectra of 30 kVp for (a) Mo/Mo, (b) Mo/Rh, (c) Rh/Rh and (d) W/Rh target/filter combination (NCRP, 2005)

The proposed kVp range varies among different studies. For example, 24-32 kVp was proposed by the International Atomic Energy Agency (IAEA) while Zhang et al. (2012) considered 18-42 kVp a suitable range for traditional mammography. In a related study by Ranger et al. (2010), 23–35 kVp was used. In general, mammography procedure utilizes x-ray beam in the range of 25-40 kVp to acquire digital images of the breast (Antunes et al., 2018). Mammography systems are designed in such a manner that they display the compressed breast thickness (CBT) during examination. This, along with the breast density are the major factors that

determine the kVp used (Sprawls, 1995). The kVp can be selected manually based on experience or an established technique chart. Alternatively, kVp selection could be done automatically based on breast characteristics.

2.1.1(b) Interaction of x-ray with matter

When x-rays interact with matter, they are either transmitted, absorbed, or scattered. These processes are referred to as attenuation. There are 2 major methods through which attenuation occur namely, Photoelectric effect and Compton scattering. Photoelectric effect is the predominant form of interaction in mammography because it involves the use of low photon energy. In photoelectric effect, an incoming photon interacts with a tightly bound inner shell electron. The photon transfers all its energy to the electron, thereby overcoming its binding energy and ejecting the electron from its shell. The ‘hole’ created in the inner shell due to the ejection is filled by an electron from the outer shell. The loss in energy of the outer shell electron in this process releases a characteristic x-ray photon. The ejected electron only travels a small distance and deposits its energy into the surrounding matter. The released photon possesses very small energy and is absorbed instantly with the release of a further, low-energy or "Auger" electron and all the energy is said to have been absorbed by the material.

2.1.2 Image acquisition and parameters

The physics of x-ray image acquisition in mammography could be illustrated through a simple model of a breast containing a lesion as seen in Figure 2.3. This model demonstrates the reason for the use of low energy -ray spectrum in mammography. x-rays transmission through the breast tissue are attenuated differently due to the variation in densities of adipose and fibro glandular tissues within the breast. Figure 2.3 demonstrates two typical paths; A and B, that the monoenergetic x-ray beam can travel. In path A, the x-ray passes through the normal breast tissue. While in path B, the x-ray passes through the portion of the breast with an embedded structure (lesion) of thickness ‘a’.

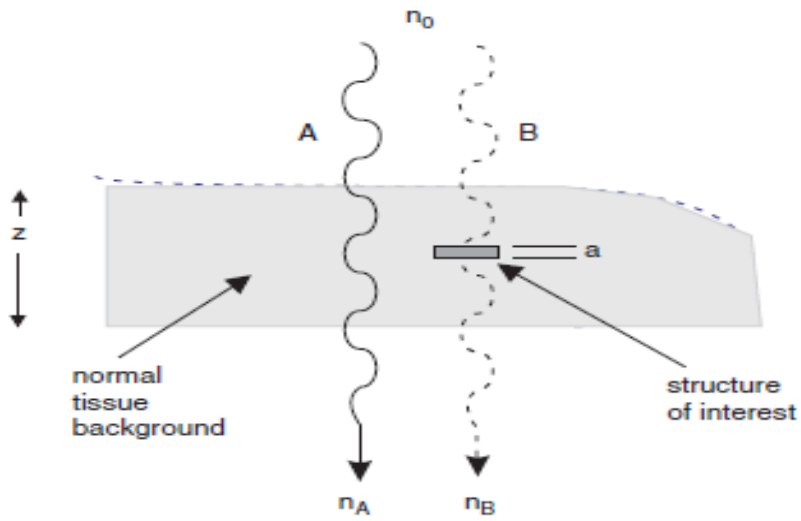

Figure 2.3 Schematic diagram of the breast showing x-ray transmission path A: through normal breast tissue, B: through structure of interest (Yaffe, 2010a).

The mean number (n_A) of the monoenergetic x-ray beam transmitted through the breast tissue along path A is given by Equation 2.1.

$$n_A = n_0 e^{-\mu z} \qquad 2.1$$

where n_0 is the mean number of x-rays incident on the breast, μ is the linear attenuation coefficient of the breast tissue and z is breast thickness.

The mean number (n_B) of monoenergetic x-ray beam transmitted through the lesion of thickness 'a' is given by the Equation 2.2.

$$n_B = n_0 e^{-\mu(z-a)-\mu' a} \qquad 2.2$$

Where μ′ represents the x-ray attenuation coefficient of the lesion. The signal difference produced between n_A and n_B can be evaluated using Equation 2.3.

$$SD = n_A - n_B \qquad 2.3$$

The resultant contrast can be defined as Equation 2.4

$$\frac{n_A - n_B}{n_A + n_B} \qquad 2.4$$

Substituting Equations 2.1 and 2.2 into Equation 2.4 yields Equation 2.5

$$\frac{1 - e^{-(\mu-\mu')a}}{1 + \varepsilon^{-(\mu-\mu')\propto}} \qquad 2.5$$

Equation 2.5 shows that contrast is a function of the difference in x-ray attenuation coefficient between the background breast tissue and the lesion and the thickness of the lesion. The contrast is not related to the thickness of the breast (*z*), the mean number of transmitted x-ray beam to the breast (n_0), and the x-ray attenuation coefficient (μ) in this simplified model. However, in practice, with the polyenergetic x-ray spectrum, where some scattered radiations are recorded, the contrast depends on *z*, n_0 and μ (Yaffe, 2010a).

2.1.3 Mammography density

Mammographic density could be defined as the percentages of fibro glandular (stroma and epithelial cells) and adipose tissues that constitutes the breast (Ding & Molloi, 2012). Mammary density is not perceived by palpation; it is rather related to the appearance of breast images on mammograms. The x-ray attenuation coefficient of fibro glandular tissue is higher than that of the fatty tissue present in the breast, therefore, the relative amounts of fibro glandular tissue determine the radiographic appearance of the breast on a mammogram. White (radio dense) areas on the mammogram represent the fibrous and glandular tissues in the breast, whereas, the dark (radiolucent) areas represents the less dense adipose tissue (Hooley et al., 2012; Subashini et al., 2010; Ursin & Qureshi, 2009).

2.1.3(a) Breast Imaging Reporting and Data System (BIRADS)

The Breast Imaging Reporting and Data System (BIRADS) developed by the American College of Radiology (ACR) classified breast density into four categories.

The categorization was done based on the ratio of fibro glandular-to-adipose tissue composition in breast. Category A breast is almost entirely fat (< 25% fibro glandular tissue), Category B contain scattered areas of fibro glandular tissue (25 – 50% fibrous tissue), Category C breast are heterogeneously dense (50 - 75% fibro glandular tissue) and Category D is extremely dense breast containing more than 75% fibro glandular tissue. Figure 2.4 show the breast density classification according to BIRADS as documented by ACR (American College of Radiology, 2013).

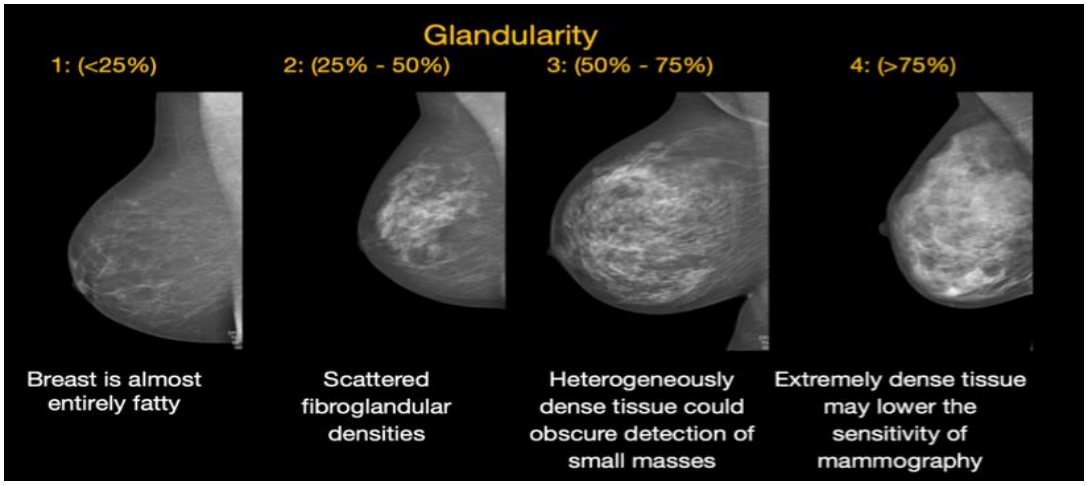

Figure 2.4 Breast density classification according to BIRADS (American College of Radiology, 2013)

2.1.4 Digital mammography

Following publication of the Digital Mammographic Imaging Screening Trial (DMIST) in 2005 (Pisano et al., 2005) mammography facilities gradually began shifting from screen-film mammography (SFM) to digital mammography (DM) (van Ravesteyn et al., 2015). According to Brooks & Morley (2013), DM was carried out progressively in Canada in 2006 and has been widely used in recent years. The full-field digital mammography (FFDM) was first approved by the U.S Food and Drug Administration (FDA) for clinical purposes in 2000 (Hendrick et al., 2010). Mammography procedures based on direct digital radiography (DR) rather than computed radiography (CR) was embraced by the Department of Health Advisory

Committee on Breast Cancer Screening in the UK in 2010. As at October 2013, over 99% of the breast screening facilities in the UK were already equipped with at least one direct digital mammography unit (Public Health England, 2014).

Digital mammography (DM) is classified into two; computed radiography (CR) and digital radiography (DR). In comparison with its analogue counterpart, screen film mammography (SFM), DM has some advantages. While the film used in SFM serve as both the detector and the display, in DM these are different devices, allowing each stage of the imaging process (acquisition, pre-processing, post-processing and display), to be optimised independently of the others (Diffey, 2015).

Generally, CR systems employ the use of imaging plates and a separate reader. On the other hand, the direct digital radiography (DR) systems have an inbuilt x-ray system and detector. The image in a DR system is displayed on the computer instantly after the x-ray exposure. Past studies have shown that CR is cheaper and less effective in detecting cancer lesions compared to DR. Bosmans et al. (2013), in a study to compare the technical and clinical screening performance parameters between CR and DR systems using technical and patient dose survey data of 25 CR and 37 DR systems concluded that the radiation doses employed for CR are 60% greater than for DR. In a cohort study carried out among European women aged 50 - 74 years screened with DR, CR or SFM between 2008 - 2009. Performance was compared between cohorts, with SFM as the referent cohort. Statistical analysis showed that inasmuch as DR is equivalent to SFM for breast screening among women aged 50 – 74 years, the rate of cancer detection with CR was much lower. This lower effectiveness could be as a result of loss of spatial resolution, or sharpness, and image noise (Brooks & Morley, 2013; Chiarelli et al., 2013).

2.1.5 Detectors for digital mammography

The detector is one of the vital components of a digital mammography system. It produces electronic signal that represents the spatial pattern of x-ray transmitted by

the breast. The detector is configured to overcome some of the drawback associated with the screen-film image receptor used in SFM, thereby, potentially yielding improved diagnostic image quality and a reduction of dose to the breast (Yaffe, 2010b). The detector interacts and absorbs the x-rays transmitted by the breast. The x-ray energy is converted to light or electronic charge signal. The light signal generated by phosphor-based detectors are further converted to electronic charge. This signal is collected, readout, followed by amplification and digitization. There are two category of digital mammography detectors: direct and indirect detectors. In direct digital detectors, the x-ray photons are absorbed by the detector and further converted directly into electric signal as a result of the presence of an electric field. On the other hand, the indirect detectors convert x-ray photon to light first before converting to electric signal. There is increasing evidence to suggest that differences in detector technology are associated with variations in cancer detection rate, dose, and image quality (Diffey, 2015). Figure 2.5 shows the detector technologies employed in analogue and digital mammography.

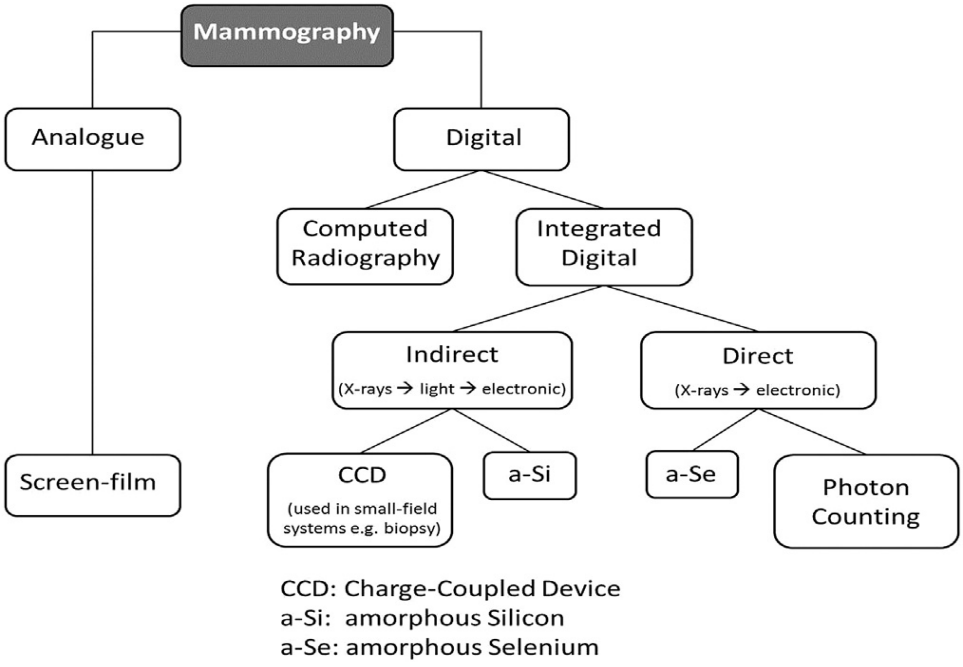

Figure 2.5 Detector technologies employed in analogue and digital mammography (Diffey, 2015).

2.1.6 Breast anatomy and properties

2.1.6(a) Anatomy

The female breast (Figure 2.6) is a tear shaped organ that spreads across the pectoralis major muscles and usually extend from the level of the second rib to the level of the sixth rib in the front of the human rib cage. The breast tissue is held in place by fibrous connective tissue known as the suspensory Cooper's ligaments. This ligament helps to connect the breast to the chest muscle and maintain its shape. The breast is composed of various layers of tissue, majorly the adipose tissue and glandular tissues. The glandular portion of the breast consists of 14 -18 irregular lactiferous lobes separated by fat and each lobe is made up of several lobules. Each lactiferous lobe has a major duct that connects it to the nipple. The lobules are composed of alveoli cells which surrounds fine tubes called ductules. The ductules join to each other to form a larger tube called a lactiferous duct. The milk produced in the alveoli flows to the nipple through the lactiferous duct.

The dimensions, weight, and the ratio of tissue composition of the breast differ among women. A typical female breast weighs roughly between 500 to 1,000 grams. The adipose-to-fibroglandular tissue ratio determines the density or firmness of the breast. Due to hormonal changes during puberty, menstrual cycle, pregnancy, breastfeeding, and menopause, the female breasts undergo changes in size, shape, and weight during her lifetime (Grassley, 2002; Pamplona & de Abreu Alvim, 2004). The size of the breast depends majorly on the amount of the adipose tissue in the breast. Usually, smaller breasts have a higher amount of glandular tissue compared to their adipose tissue (Fritsch et al., 2007).

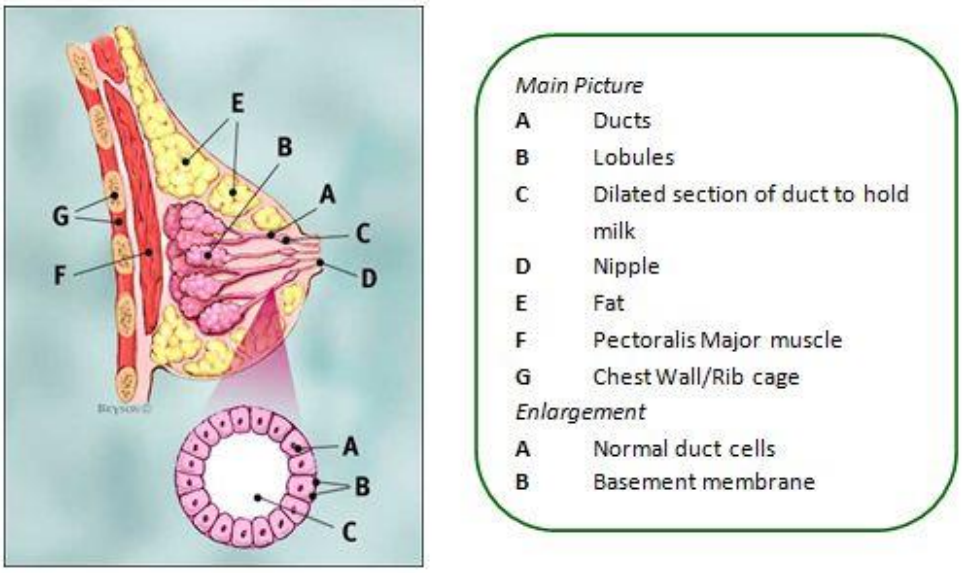

Figure 2.6 Anatomy of the breast (Marshall University, 2020)

2.1.6(b) Physical properties

The density and atomic number of the elements that make up the tissue are useful physical quantities in medical imaging and radiotherapy. These parameters in addition to the peak kilovoltage determine the level of x-ray interaction with tissues and hence the rate of differential absorption. The mass density (ρ) of any substance is defined as the quantity of matter present in that substance. It is the ratio of mass to volume of a given material. Various tissues have different densities depending on their elemental composition. If we think of mass density as how tightly the atoms are packed, thicker body parts with higher densities would have greater chance of interaction. About 99% of the entire mass of the human body is composed of oxygen, carbon, hydrogen, nitrogen, calcium, and phosphorus. Approximately 0.85 % is made of potassium, sodium, sulphur, chlorine, and magnesium. These elements are all necessary for life. The rest are trace elements, which are also useful for life.

The photoelectric effect has some vital implication in medical imaging. In diagnostic radiology, the primary mode of interaction is photoelectric. It is also responsible for the contrast effect. Imaging an area with bone and soft tissue have

higher differential absorption because of the difference in atomic number than an area of strictly soft tissue where all the atomic numbers are relatively the same.

2.1.6(c) Radiological properties

Radiation from x-rays and/or gamma rays are largely employed in diagnostic and therapeutic radiology, understanding of the details of interaction of ionizing radiation with the human tissue becomes very crucial from the point of dosimetry and radiological protection. Therefore, correct values of photon interaction parameters like the effective atomic number (Z_{eff}) and electron density (ρ_e) are needed to provide decisive information on photon interaction with target material.

The atomic number Z of any elements, can be linked with the basic properties of that element, as described by the well-known Moseley's law (Moseley, 1913). As for multi element materials, the Z_{eff} is used to describe the basic radiation interaction properties of different compounds or mixtures (Taylor et al., 2012b). On the other hand, the ρ_e refers to the number of electrons per unit mass of a multi element material. Both parameters vary with photon energy.

In radiation dosimetry, tissue substitute or phantoms are commonly used to estimate the radiation dose received by patients. For any material to be considered as tissue equivalent, it must have Z_{eff} and ρ_e values similar to those of the tissue they mimic (Kurudirek, 2016; Kurudirek, 2014a). The Z_{eff} represents the properties of composite materials consisting of distinct elements in various proportions mostly in the radiation field depending on atomic numbers of the constituent elements and incident radiation energy (Kurudirek, 2014a). It shows the number of electrons of the composite material that are actively involved in the photon–atom interaction. Thus, this parameter is constantly used for the calculations of mass energy absorption coefficients and Kerma in radiation dosimetry, it also finds application in medical physics, radiation dosimetry, radiation biology, radiotherapy, and nuclear industry. Since Z_{eff} is ascertained by considering the weight of different partial radiation

interaction processes at different energies, this parameter is therefore viewed as energy dependent. For this reason, Z_{eff} ought not to be represented by a single number as opposed to elements that have a single atomic number.

Apart from being energy dependent, Z_{eff} also varies with respect to the chemical composition of the material considered. Hence, it is an important parameter that reveals how radiation interacts with different types of materials in the entire energy region (Murat Kurudirek, 2014b). Z_{eff} is one of the reliable parameters to determine the suitability of a composite material for use as phantoms (Kore & Pawar, 2014; Murat Kurudirek, 2014b; Larsson et al., 2015; Taylor et al., 2012a; Turşucu et al., 2013; Yusof et al., 2017). The most common method used by researchers to evaluate Z_{eff} is the simple power law by Mayneord (Mayneord, 1937). This historic approach is used for many applications and was derived for a monoenergetic X-ray source. Consequently, it provides a single value of Z_{eff} for any material for low energy photons for which photoelectric absorption is the dominant interaction process.

Even though researchers are aware of the limitations associated with the use of Mayneord's formula as a simple means of Z_{eff} calculation, many of them would still employ this method to avoid the relative complexities of the more rigorous energy-dependent computations (Taylor et al., 2012). Admitting this challenge, some studies have developed useful software that enable the calculation of Z_{eff} across a wide energy range, they include the Auto Z_{eff} and Phy-X/ZeXTRa computer programs (Ozpolat et al., 2020; Taylor et al., 2012b). The Phy-X/ZeXTRa is a new online software developed by Ozpolat et al. (2020) for the robust calculation of Z_{eff} for photon, electron, proton, alpha particle and carbon ion interactions. Given the necessary information about the mole fraction or weight fraction of mixtures and compounds, this software enables a swift, accurate and simultaneous calculation of Z_{eff} for the composite materials at different energies. This user friendly graphical user

interface (GUI) program evaluates Z_{eff} for photon in the energy range of 1 keV–20 MeV, and for electrons, protons, alpha particles and C ions in the energy range of 1 MeV–1 GeV (Ozpolat et al., 2020).

2.1.6(d) Attenuation properties of breast tissue

X-ray attenuation is produced by the absorption and scattering of photons. The x-ray attenuation properties of some body parts, such as breast tissue, can be measured by the value of linear attenuation coefficient (μ), mass attenuation coefficient (μ/ρ) and computed tomography (CT) number.

The linear attenuation coefficient is the basic quantity that determine the attenuation properties of a material towards ionizing radiations. It measures the ratio of the transmitted to the initial photon intensity as the photon travels through a medium. When a monoenergetic photon travels through a medium with thickness x, its intensity will be attenuated and reduced by the medium according to Beer-Lambert's law which is given by Equation 2.6

$$I = I_0 e^{-\mu x} \qquad 2.6$$

where I_0 and I are the initial and final intensity of photon, and μ is the linear attenuation coefficient of sample in cm^{-1}. The linear attenuation coefficient of a sample can be calculated by modifying Equation 2.6 into 2.7

$$\mu = \frac{1}{x} ln \frac{I_0}{I} \qquad 2.7$$

The density independent mass attenuation coefficient is the ratio of μ to the density (ρ) of the sample as expressed in Equation 2.8.

$$\mu/\rho = \frac{1}{\rho x} ln\left(\frac{I_0}{I}\right) \qquad 2.8$$

Past studies have demonstrated that the measured attenuation coefficient of the breast components; fat, fibro glandular tissue and lesions (Figure 2.7) decrease with increased x-ray energy (Yaffe, 2010a). This is because the higher energy photons are less likely to interact, and subsequently be attenuated by the tissue. Consequently, radiation contrast will decrease with increasing x-ray energy. The desire to achieve an adequate radiation contrast between the breast tissue and embedded lesion is the basis for employing relatively low x-ray energies in mammography (Figure 2.8) (Yaffe, 2010a). Table 2.2 show the values of physical and radiological properties of breast tissue and calcification.

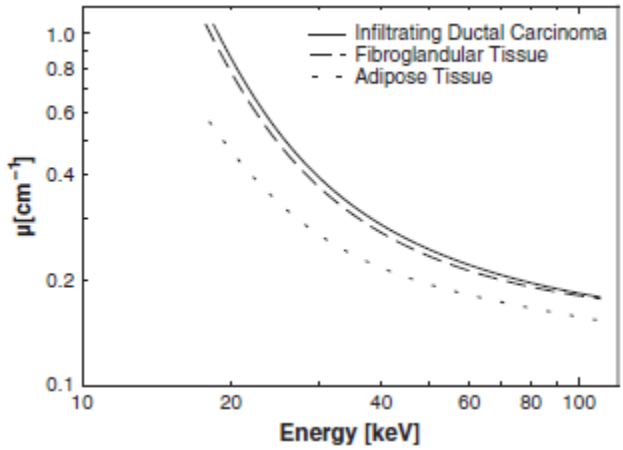

Figure 2.7 Linear x-ray attenuation coefficients of fat, fibroglandular tissue, and tumour in the breast (Yaffe, 2010a).